ACS OMEGA

http://pubs.acs.org/journal/acsodf

Article

Study on Preparation and Properties of Ultrahigh Molecular Weight Polyethylene Composites Filled with Different Carbon Materials

Yuantao Zhao,[⊥] Tao Jiang,[⊥] Ying Wang,[⊥] Xinfeng Wu,* Pingkai Jiang, Shanshan Shi, Kai Sun, Bo Tang, Wenge Li,* and Jinhong Yu*

Cite This: *ACS Omega* 2022, 7, 5547−5557

Read Online

ACCESS | Metrics & More | Article Recommendations

ABSTRACT: The development of ultrahigh molecular weight polyethylene (UPE) has been restricted due to its linear structure and low thermal conductivity. In this paper, graphene oxide (GO) was prepared by the modified Hummers method, and then UPE/reduced graphene oxide (rGO) powder was prepared by reduction with hydrazine hydrate. UPE/natural graphite (NG), UPE/carbon nanofiber (CNF), and UPE/rGO are prepared by hot compression molding. With the increase of thermally conductive fillers, the high density of the composite makes the thermal conductivity of the crystal structure more regular and the thermal conductivity path increases accordingly. Both TGA and SEM confirmed the uniform dispersion of carbon filler in epoxy resin. Among the three composites, UPE/NG has the best thermal conductivity. When the NG filling content is 60 phr, the thermal conductivity of the UPE/NG composite is 3.257 W/(mK), outperforming UPE/CNFs (0.778 W/(mK) and pure UPE (0.496 W/(mK) by 318.64 and 556.65%, respectively. UPE/CNFs have the best dielectric properties. Comparison of various carbon fillers can provide some references for UPE's thermal management applications.

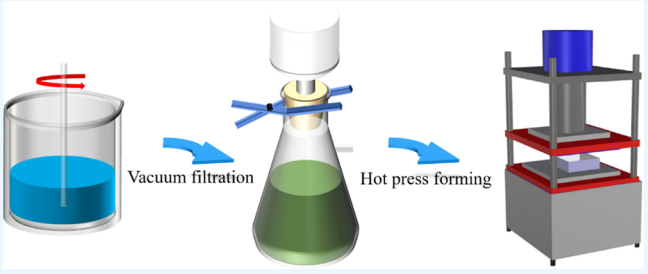

1. INTRODUCTION

Ultrahigh molecular weight polyethylene[1,2] (UPE) has a highly entangled molecular chain due to its ultrahigh molecular weight, and this structure makes UPE-based composites have good wear resistance,[3,4] impact resistance,[5,6] corrosion resistance,[7,8] and other properties.[9,10] It is used in the fields of mechanical parts, marine cables, weapon shells, radar protective shell covers, and so forth. However, at the same time, the intrinsic thermal conductivity of UPE is very poor, and it cannot be used in some thermal and heat dissipation fields.[11,12] If the thermal conductivity of UPE-based polymers can be improved while retaining its unique properties, the application range of UPE will be greatly broadened. Therefore, it is of great practical significance to improve the thermal conductivity of UPE.[13−15]

The main ways to improve the thermal conductivity of polymer composites include modifying the resin to increase the intrinsic thermal conductivity,[16,17] adding thermally conductive fillers[18,19] such as natural graphite,[20,21] carbon nanofibers (CNF),[22,23] reduced graphene oxide (GO),[24,25] carbon fiber,[26] and so forth, and reducing the interface thermal resistance.[27,28] Adding thermally conductive fillers is the most direct and effective way to improve the thermal conductivity of materials. Graphite has superior electrical and thermal conductivities due to its dense carbon crystal accumulation structure. Feng[29] et al. prepared a highly anisotropic polyolefin elastomer/NG composite through the method of two-roll mill without any magnetic and electric fields. When the addition amount of NG is 49.3%, the thermal conductivity of the composites can reach 13.27 W/(mK), which shows that the addition of NG can indeed improve the thermal conductivity of the polymer-based composites. CNF[30,31] can be used in the preparation of polymer-based thermally conductive composites because of its higher degree of crystal orientation and better electrical conductivity. Ma[23] et al. prepared graphene nanoplatelets/CNFs/EP composites by simple suction filtration; the thermal conductivities are 3.74 W/(mK) in the radial direction and 3.28 W/(mK) in the axial direction, at filler contents of 13.09 and 14.49 wt %, respectively. Mazo[22] et al. through spark plasma sintering prepared CNFs/SiOC composites with different contents. The addition of 1% CNFs increased the thermal conductivity of the composites by 30% and the electrical conductivity by 3 orders of magnitude. This shows that the addition of CNF has a significant impact on the thermal and electrical conductivity of the composites.

Received: December 12, 2021
Accepted: January 21, 2022
Published: February 2, 2022

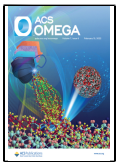

https://doi.org/10.1021/acsomega.1c07023
ACS Omega 2022, 7, 5547−5557

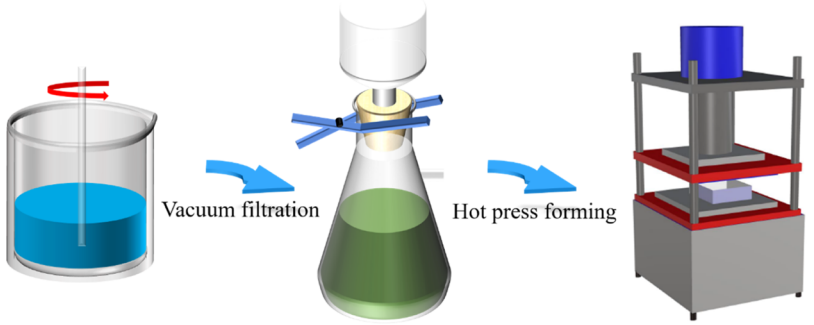

Figure 1. Schematic diagram of the preparation of UPE/NG and UPE/CNF composites.

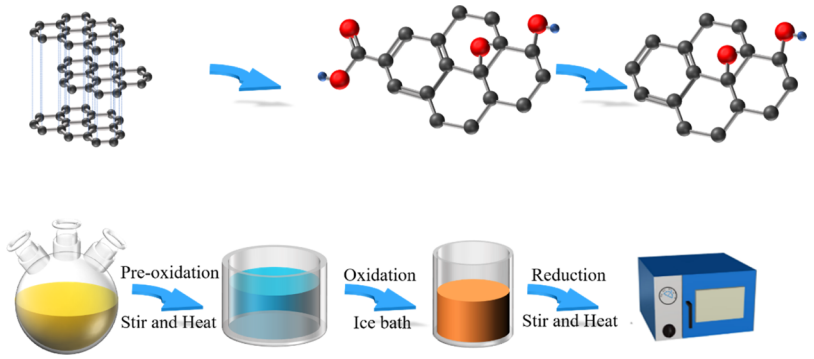

Figure 2. Schematic diagram of the preparation of UPE/rGO composites.

Graphene[32,33] has excellent thermal conductivity and electrical conductivity due to its unique sp^2 large π bond conjugated planar structure, and its thermal conductivity is as high as 5300 W/(m·K), which is higher than that of carbon nanotubes and diamonds. Reduced graphene oxide (rGO) loses many functional groups during the reduction process, so its properties become more stable. Jin[34] et al. added rGO as an additive to aramid nanofibers to improve the thermal conductivity of the composites. 40% rGO addition can increase the thermal conductivity of aramid nanofibers by 1250%. Liu[35] et al. added rGO to the silver nanoparticle-decorated boron nitride hybrid to prepare a thermally conductive framework by hydrothermal treatment and then compounded it with PDMS to obtain a thermally conductive polymer. The thermal conductivity test results showed that the addition of rGO effectively enhanced the thermal conductivity and electrical conductivity of the composites. In summary, the addition of NG, CNF, and rGO carbon fillers will have a certain impact on the thermal and electrical conductivity of polymer composites. Therefore, in this paper, three carbon materials are added to UPE, and the changes in properties such as thermal conductivity and electrical conductivity of UPE-based composites are studied.

In this paper, GO was first prepared by the modified hummers method, and then GO was reduced by hydrazine hydrate. Three types of composites, UPE/NG, UPE/CNF, and UPE/rGO, were prepared using ethanol solution mixing and hot pressing. The results show that the thermal conductivity of UPE/NG is the best, up to 3.257 W/(mK) (60 phr NG), which is 556.7% higher than the thermal conductivity of pure UPE. Both SEM and TGA proved the uniformity of filler dispersion. UPE/CNF has the best electrical conductivity. The addition of carbon materials shows the application potential of UPE in the field of thermal management.

2. EXPERIMENTAL SECTION

2.1. Experimental Materials. UPE was obtained from Shanghai Lianle Chemical Technology Co., Ltd (Shanghai, China), with a maximum particle size of 250 μm. The NG powder was purchased from Qingdao Xinghe Graphite Co., Ltd (Shandong, China), with an average particle size of about 30 μm and a purity of 99.85%. CNF was obtained from Showa Denko, Japan. DMF, $KMnO_4$, $K_2S_2O_8$, P_2O_5, and H_2SO_4 (98%) were all purchased from Shanghai Lingfeng Chemical Reagent Co., Ltd. $BaCl_2$, HCl, C_2H_5OH, H_2O_2 (30%), and $N_2H_4{\cdot}H_2O$) (60%) were purchased from Sinopharm Chemical Reagent Co., Ltd. Deionized water was made in the laboratory.

2.2. Preparation of UPE/NG and UPE/CNF Composites. Figure 1 shows the schematic diagram of the preparation of UPE/NG and UPE/CNF composites. The preparation process is mainly divided into three steps. First, the UPE/NG mixed powder and UPE/CNF mixed powder are dispersed uniformly in ethanol solution in a certain proportion. Second, the obtained mixed powder ethanol solution is vacuum-filtered and dried. Finally, the mold (10 cm × 10 cm × 1 mm) is preheated to a certain temperature (200 °C); then a certain amount of premixed UPE-NG composite powder is weighed into the preheated mold for hot pressing.

2.3. Preparation of UPE/rGO Composites. Figure 2 shows the schematic diagram of the preparation of UPE/rGO composites. The preparation of composites is mainly divided into two steps. The first step is to prepare the UPE/rGO mixed powder. The preparation of rGO can be divided into three parts: preoxidation, oxidation, and reduction. The three-neck flask is used for preoxidation, and the natural graphite powder is preoxidized by heating and stirring to obtain preoxidized graphite. The obtained preoxidized graphite is continuously oxidized in an ice bath and then subjected to centrifugal washing to obtain GO. Then, the UPE powder and GO are

https://doi.org/10.1021/acsomega.1c07023
ACS Omega 2022, 7, 5547−5557

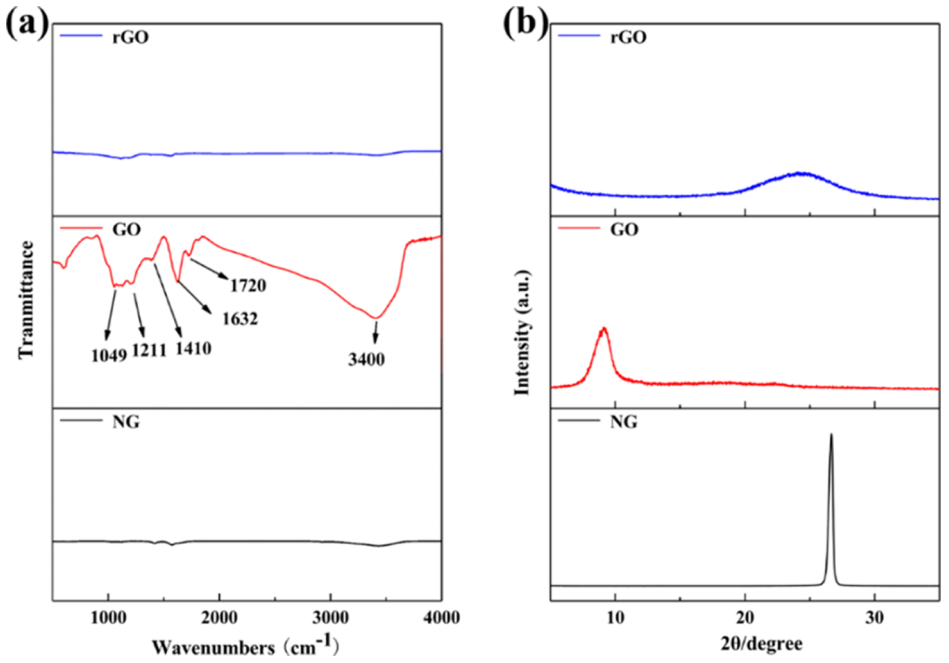

Figure 3. (a) FTIR and (b) XRD of NG, GO, and rGO powder.

mixed in ethanol solution, hydrazine hydrate is added to reduce the GO, and the UPE/rGO mixed powder can be obtained after vacuum drying. The second step is to use a hot press for hot pressing.

2.4. Characterization. Characterization of NG, GO, and rGO powders is performed by XRD, FTIR, and TGA. The scanning speed of the XRD test is 5°/min, and the scanning range is 5−30°. The SEM, TGA, DTG, DSC, density, thermal conductivity, and dielectric properties of the three composites of UPE/NG, UPE/CNF, and UPE/rGO were characterized. Among them, the DSC test is carried out in a nitrogen atmosphere, with a heating rate of 10 °C/min, scanning from 20 to 200 °C, and the sample weight is 5−10 mg. The frequency range of the dielectric performance test is 10^{-1} to 10^{6} Hz. To test the AC conductivity of the composites, both sides of the sample need to be sprayed with gold. The four-probe method was used to test the DC conductivity of the composites.

3. RESULTS AND DISCUSSION

3.1. Characterization of NG, GO, and rGO Powder. Figure 3 shows the FTIR and XRD of NG, CNF, and rGO powder. It can be clearly seen from Figure 3a that there is almost no absorption peak on NG, which shows that there are no active groups. GO is obtained after NG is oxidized. Many new peaks appear on the FTIR spectrum. The assignment of each new peak is as follows: 1632 cm^{-1} is the stretching vibration peak of the carbon−carbon double bond (C═C), which is very sharp, 1720 cm^{-1} is the stretching vibration peak of the carbonyl group (>C═O), 1211 cm^{-1} is the stretching vibration peak corresponding to the alkene ether or aromatic ether part (═C−O−), 1049 cm^{-1} is the absorption peak of stretching vibration of fatty ether (═C−O−C), and 1410 cm^{-1} is the O−H plane variable angle vibration peak associated with hydrogen bonding. The absorption peak at 3400 cm^{-1} is large and wide. This is because after the natural graphite flakes are oxidized into GO, the surface contains a large number of hydrophilic groups, which can easily absorb water. The absorption peak is the stretching vibration absorption peak of a large number of water molecules adsorbed by GO. The appearance of a large number of new functional groups in GO indicates that NG has been fully oxidized. After GO was reduced to rGO by hydrazine hydrate, all the peaks of the oxidized groups almost disappeared, indicating that the reduction effect of hydrazine hydrate was still very good. During the oxidation−reduction process of NG, the interlayer spacing of graphite will change accordingly. The larger the interlayer spacing of the graphite layer, the smaller the corresponding diffraction angle. It can be seen from Figure 3b that the diffraction angle of NG is 26.6°, and the peak intensity is very strong and sharp, indicating that the graphite sheet structure of natural graphite material is arranged unconventionally. The diffraction angle of GO is about 9.1°. This is because after the NG is oxidized, the graphite interlayer is oxidized and destroyed, especially from the edge position and becomes carbonyl (>C═O), carboxyl (−COOH), hydroxyl (−OH), and other molecular structures (Figure 3a), that is, the hybrid structure of the graphite layer changes from sp^2 to sp^3, the graphite layer is stretched, and the interlayer spacing increases, so the diffraction angle then becomes smaller. Oxidation will destroy the original ordered structure of NG.

Figure 4 shows the TGA curve of NG, GO, and rGO. It can be seen from the figure that NG has almost no weight loss before 600 °C, and the material maintains very good thermal stability. The weight loss is only 18.8% even under the 700 °C air atmosphere, and this may be the weight loss caused by the impurities adsorbed in the natural graphite. The weightlessness curve of GO is divided into several stages: the first stage is from 50 to 145 °C, where the sample loses 12%, which is mainly caused by the evaporation of water in the sample. The second stage is 145−302 °C, where the sample weight loss is 38%. The main reason is that the oxygen-containing groups on the GO sheet, such as carboxyl, carbonyl, and hydroxyl groups, are oxidatively degraded and converted into small molecular gases such as carbon dioxide. The weightless group can be

https://doi.org/10.1021/acsomega.1c07023
ACS Omega 2022, 7, 5547−5557

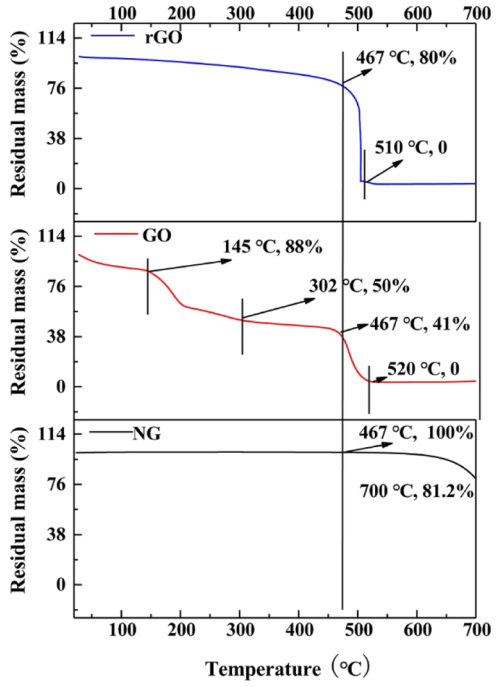

Figure 4. TGA of NG, GO, and rGO powder.

verified from the infrared spectrum at the front, which shows that the content of oxygen-containing groups in GO is very high. The third stage is 302−467 °C; this stage is relatively gentle, and weight loss is about 9%, which is caused by the oxidative degradation of refractory degradable groups such as carbon−carbon double bonds. The fourth stage is from 467 to 520 °C, and the degradation is relatively severe. The remaining samples are completely degraded with a weight loss of 41%, which is mainly caused by the oxidative degradation of the six-membered carbocycle skeleton structure. Compared with natural graphite, GO has more skeletal structure defects, which leads to a decrease in thermal stability. rGO has a two-stage degradation process: the first stage is from 50 to 467 °C, the sample loses 20% in weight, and the whole process is slow. Although GO becomes rGO after being reduced by hydrazine hydrate, some defects are unavoidable. It is impossible to completely be a six-membered ring structure, especially at the edge. In addition, some of the defects in the middle position are easily oxidized by oxygen under high-temperature conditions and decomposed into carbon dioxide and other gases and lose weight. The second stage is 467−510 °C, and the remaining rGO is completely oxidized and decomposed. On the one hand, it is the result of the continuing effects of rGO defects, and on the other hand, it is also related to its own structure. rGO is a disordered stacked structure. Oxygen can easily invade these lamellar structures to cause an oxidation reaction, and finally, rGO is completely oxidized and decomposed. Because the natural graphite structure is an orderly and densely packed arrangement structure, oxygen is difficult to penetrate, and the material is a thin layer on the surface even if it is oxidized, so the weight loss of natural graphite is limited.

3.2. Morphology and Microstructure of Composites. Figure 5 shows the characterization of composites. It can be seen from Figure 5a that the flaky NG particles are very uniformly dispersed in the UPE matrix. Figure 5b shows that the flake-shaped NG particles are dispersed into a spherical

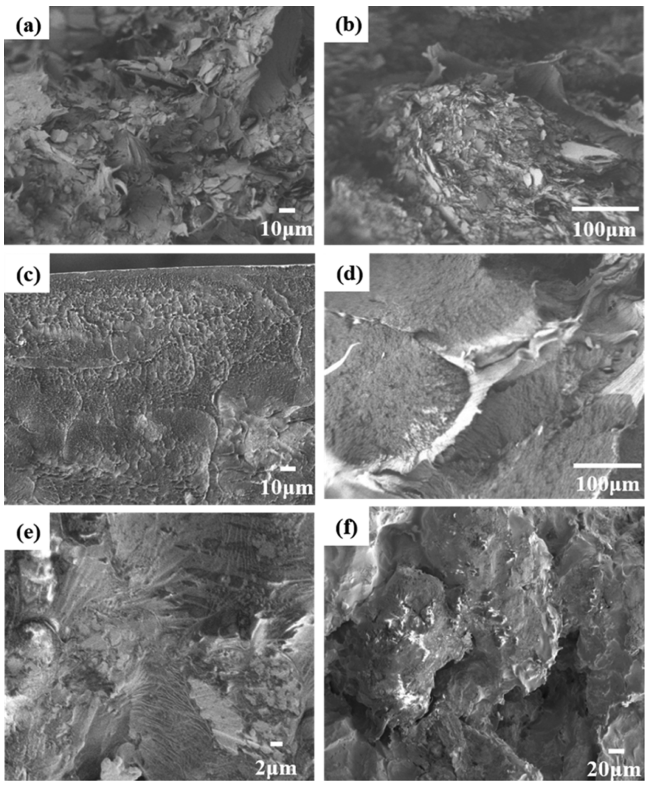

Figure 5. Characterization of composites. SEM of the UPE/NG composite with (a) 20 phr NG and (b) 60 phr NG. SEM of the UPE/CNF composite with (c) 20 phr NG and (d) 60 phr NG. SEM of the UPE/rGO composite with (e) 5 phr NG and (f) 10 phr NG.

shape to wrap the UPE powder particles. It can be seen from Figure 5c that CNF is evenly dispersed in the UPE matrix, forming a network structure. However, it is found from Figure 5d that CNF has agglomerated spheres. This may be caused by heat generation of CNF and UPE particles when the ethanol solution is ultrasonically stirred and dispersed. The agglomerated balls are like particles dispersed among the UPE particles. From Figure 5e, it can be clearly seen that the expanded rGO is uniformly dispersed in the UPE matrix. It can be seen from Figure 5f that there are many voids between the UPE particles, which may be caused by the expansion of small molecules adsorbed on the surface of rGO during the pressing process, which is not conducive to the thermal conductivity of the material.

3.3. Dispersibility and Thermal Stability of Composites. In order to further confirm the dispersibility of NG and CNF in UPE/NG and UPE/CNF composites, TGA (in N_2) was used to test the residual quality of UPE/NG and UPE/CNF composites. The residual mass is compared with the theoretical content. If the two curves overlap very well, it means that the dispersion is more uniform. Combining Figures 5b and 6a,b, it can be proved that the dispersion of NG in the UPE/NG composite is relatively uniform. From Figure 6c,d, it can be found that the dispersion of CNF in UPE/CNF composites has a certain degree of dispersion, which may be caused by the agglomeration sphere phenomenon of CNF, as shown in Figure 5d. Because rGO in UPE/rGO composites easily expands and bursts at high temperatures, TGA is not used to test UPE/rGO composites.

Figure 7 shows the DTG curve of UPE/NG and UPE/CNF composites. It can be seen from Figure 7a that the thermal

https://doi.org/10.1021/acsomega.1c07023
ACS Omega 2022, 7, 5547−5557

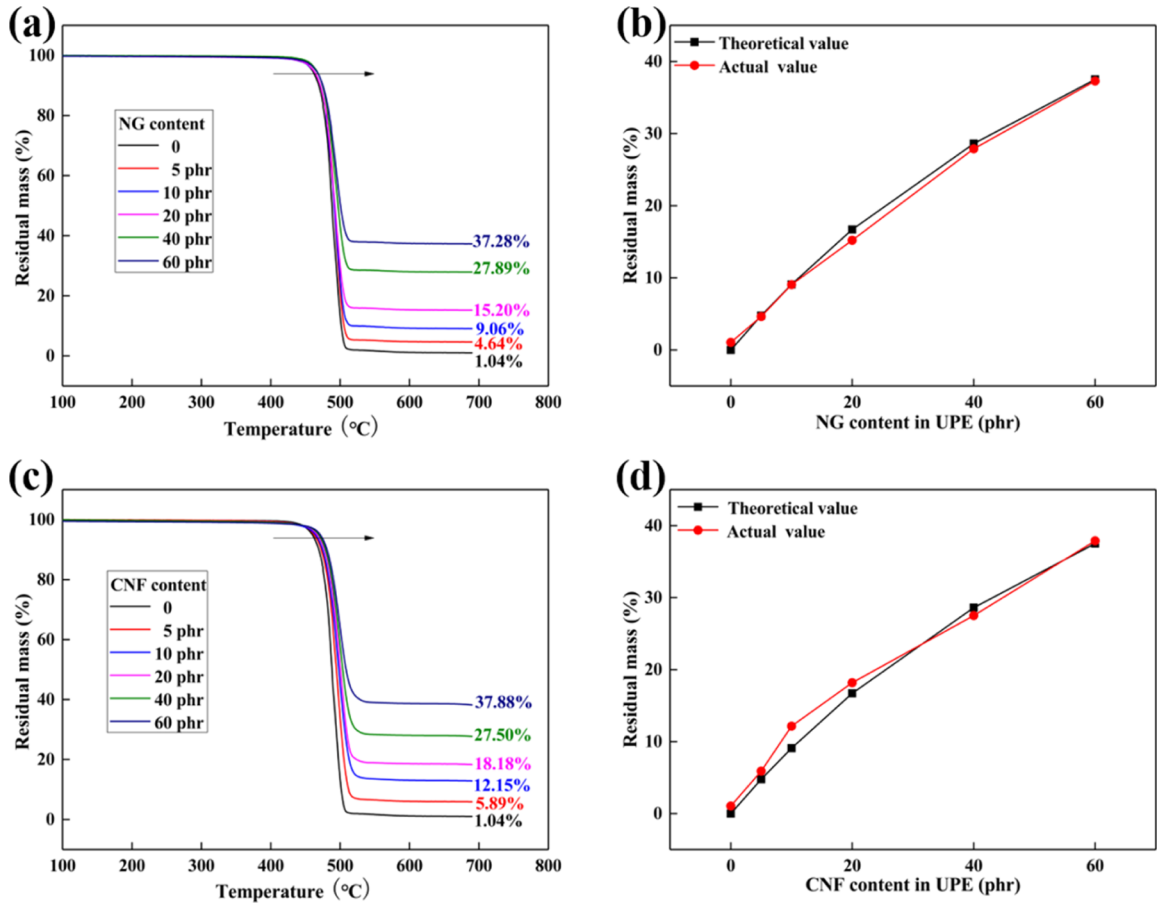

Figure 6. Comparison curve of the actual content and theoretical content of NG and CNF in UPE/NG and UPE/CNF composites. (a) Residual mass of NG in UPE/NG composites. (b) Comparison of theoretical and actual values of NG in UPE/NG composites. (c) Residual mass of CNF in UPE/CNF composites. (d) Comparison of theoretical and actual values of CNF in UPE/CNF composites.

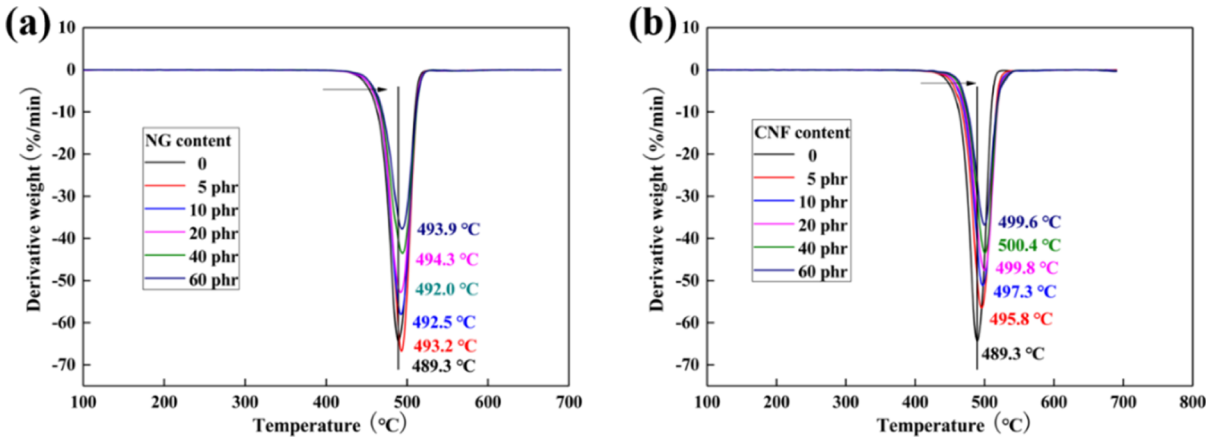

Figure 7. DTG of composites. (a) DTG of UPE/NG composites. (b) DTG of UPE/CNF composites.

stability of UPE/NG composites has increased, and the initial decomposition temperature and maximum decomposition temperature are both higher than those of pure UPE materials. In Figure 7a, the maximum decomposition temperatures of UPE/NG composites are 489.3 °C (pure UPE), 493.2 °C (5 phr NG), 492.5 °C (10 phr NG), 492.0 °C (20 phr NG), 494.3 °C (40 phr NG), and 493.9 °C (60 phr NG). The thermal stability of CNF has also increased after adding UPE. It can be seen from Figure 7b that the decomposition temperature of the UPE/CNF composites increases with the increase of CNF. The maximum decomposition temperature of UPE/CNF composites increases from 489.3 °C (pure UPE) to 495.8 °C (5 phr CNF), 497.3 °C (10 phr CNF), 499.8 °C (20 phr CNF), 500.4 °C (40 phr CNF), and 499.6 °C (60 phr CNF), and the maximum thermal decomposition temperature increased by more than 10 °C under high content. The thermal stability of the UPE/rGO composites is not discussed here because the UPE/rGO composites can burst during heating, which can easily damage the TGA instrument.

https://doi.org/10.1021/acsomega.1c07023
ACS Omega 2022, 7, 5547−5557

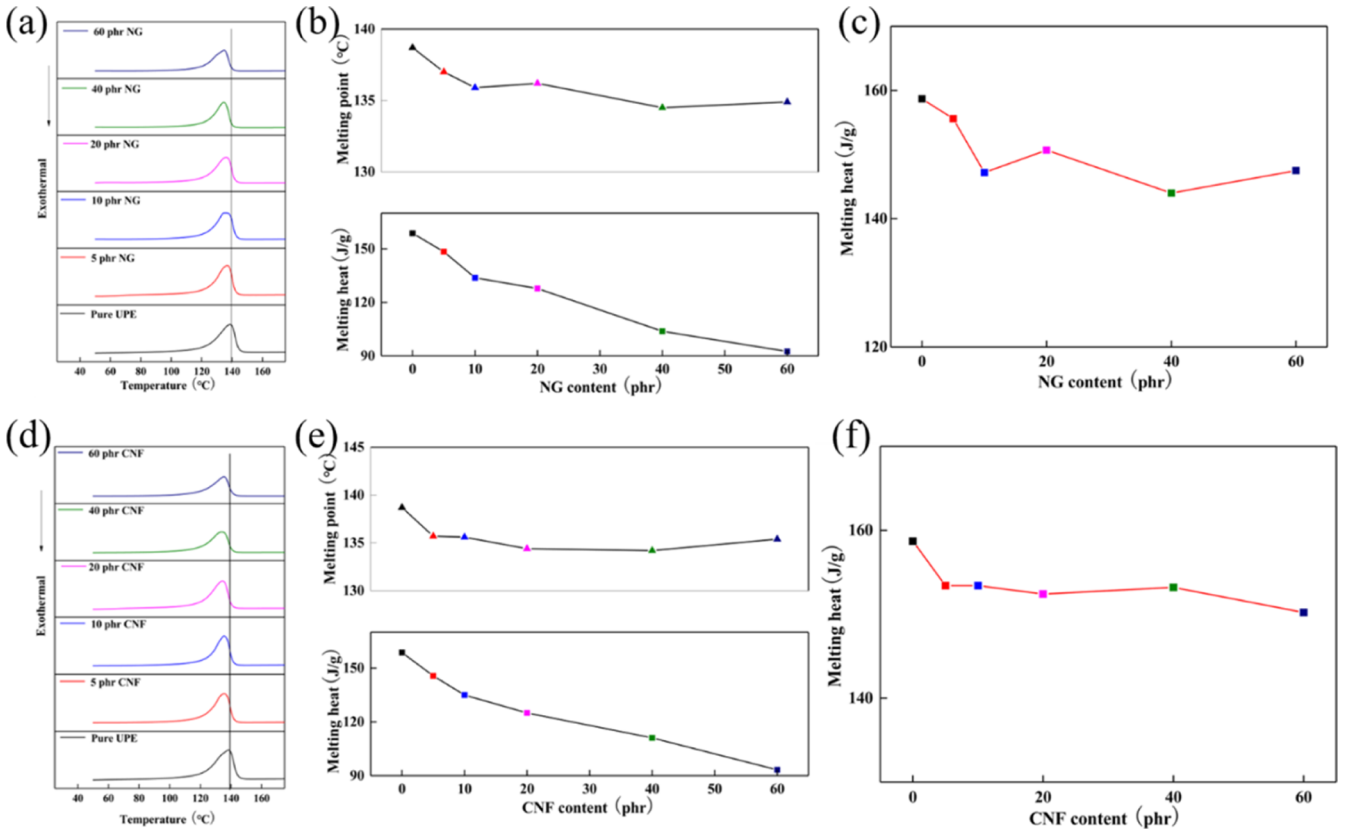

Figure 8. Melting heat and melting point of composites. (a) DSC of UPE/NG composites. (b) Melting heat of UPE/NG composites. (c) Melting point of UPE/NG composites. (d) DSC of UPE/CNF composites. (e) Melting heat of UPE/CNF composites. (f) Melting point of UPE/CNF composites.

3.4. Melting Heat and Melting Point Changes of Composites. Figure 8 shows a graph showing the heat of fusion and melting point changes of UPE/NG and UPE/CNF composites. It can be seen from Figure 8a,b that the heat of fusion of UPE/NG composites gradually decreases with the increase of NG content, and the heat of fusion decreases from 159.6 to 148.4 J/g (5 phr NG), 133.8 J/g (10 phr NG), 127.8 J/g (20 phr NG), 103.8 J/g (40 phr NG), and 92.5 J/g (60 phr NG). After the heat of fusion is converted to the actual heat of fusion, it can be seen that the actual heat of fusion has slightly decreased. It can be seen from Figure 8c that the actual heat of fusion has decreased from 159.6 to 155.6 J/g (5 phr NG), 144.2 J/g (10 phr NG), 150.7 J/g (20 phr NG), 144 J/g (40 phr NG), and 147.5 J/g (60 phr NG). The addition of NG hinders the crystallization of the UPE material, but the decrease is not too large, and the thermal conductivity of the UPE/NG composites will not be affected too much. The melting point of UPE/NG composites also decreases with the increase of NG content. The melting point decreases from 138.7 to 137.0 °C (5 phr NG), 135.9 °C (10 phr NG), 136.2 °C (20 phr NG), 136.2 °C (40 phr NG), and 134.9 °C (60 phr NG). The small decrease indicates that the crystal regularity of UPE in UPE/NG composites has decreased. The melting heat and melting point change of UPE/CNF composites are very similar to those of UPE/NG composites. The heat of fusion of UPE/CNF composites gradually decreases with the increase of CNF content. The heat of fusion decreases from 159.6 to 145.7 J/g (5 phr CNF), 135.0 J/g (10 phr CNF), 125.0 J/g (20 phr CNF), 111.1 J/g (40 phr CNF), and 93.3 J/g (60 phr CNF). After the heat of fusion is converted to actual heat of fusion, it can be seen that the actual heat of fusion has slightly decreased. It can be seen from Figure 8f that the actual heat of fusion has decreased from 159.6 to 153.4 J/g (5 phr CNF), 153.4 J/g (10 phr CNF), 152.4 J/g (20 phr CNF), 153.2 J/g (40 phr CNF), and 150.2 J/g (60 phr CNF). The addition of CNF hinders the crystallization of UPE materials, but the decline is not too large, and the thermal conductivity of UPE/CNF composites will not be affected too much. The melting point of UPE/CNF composites also decreases with the increase of CNF content. The melting point decreases from 138.7 to 137.7 °C (5 phr CNF), 137.6 °C (10 phr CNF), 134.4 °C (20 phr CNF), 134.2 °C (40 phr CNF), and 135.4 °C (60 phr CNF). The small decrease indicates that the crystal regularity of UPE in UPE/CNF composites has decreased.

Figure 9 shows the melting heat and melting point changes of UPE/rGO composites. It can be seen from the figure that the heat of fusion of the UPE/rGO composites has decreased from 159.6 J/g (pure UPE) to 141.2 J/g (5 phr rGO) and 133.6 J/g (10 phr rGO). The melting point also changed from 138.5 °C (pure UPE) to 138.6 °C (5 phr rGO) and 137.6 °C (10 phr rGO). The small changes in the heat of fusion and melting point indicate that rGO does not have much influence on the crystallization of UPE materials.

3.5. Density Changes of Composites. Figure 10 shows the density changes of UPE/NG, UPE/CNF, and UPE/rGO composites. It can be seen from Figure 10a that the density of UPE/NG increases with the increase of NG content. Density increased from 0.916 g/cm^3 of pure UPE material to 0.961 g/cm^3 (5 phr NG), 0.965 g/cm^3 (10 phr NG), 1.011 g/cm^3 (20 phr NG), 1.099 g/cm^3 (40 phr NG), and 1.159 g/cm^3 (60 phr

https://doi.org/10.1021/acsomega.1c07023
ACS Omega 2022, 7, 5547−5557

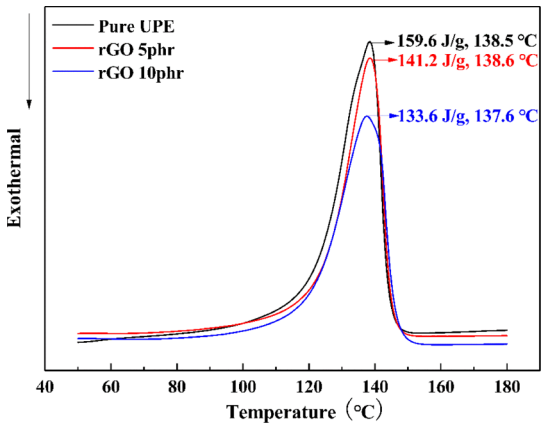

Figure 9. Melting heat and melting point of UPE/rGO composites.

NG), an increase of 4.9%, 5.3%, 10.4%, 20.0%, and 26.5%, respectively. Combined with the SEM picture in Figure 5, it can be predicted that the increase in NG content is beneficial to improve the thermal conductivity. It can be seen from Figure 10b that the density of the UPE/CNF composites increases first and then gradually decreases, but it always remains between 0.90 and 0.94 g/cm^3. This may be caused by partial agglomeration of CNF, which can be verified from the SEM images in Figure 5c,d. It can be seen from the heat conduction formulas 1 and 2 that this result is not conducive to the improvement of the thermal conductivity of UPE/CNF composites. The density of UPE/rGO composites decreases with the addition of rGO, from 0.916 to 0.835 g/cm^3 (5 phr rGO) and 0.817 g/cm^3 (10 phr rGO), which is due to the porous and loose structure formed by rGO in the UPE/rGO composite (as shown in Figure 5e,f). It can be seen from the thermal conductivity formulas 1 and 2 that the decrease in density has a negative effect on the thermal conductivity of UPE/rGO composites.

$$\rho = \frac{m_1 \rho_{water}}{m_1 + m_2 - m_3} \quad (1)$$

$$\lambda = \alpha \times C_p \times \rho \quad (2)$$

where λ, C_p, α, and ρ represent the thermal conductivity, specific heat, thermal diffusivity, and density of the composites, respectively.

3.6. Thermal Conductivity of Composites. Figure 11 shows the thermal conductivity of UPE/NG, UPE/CNF, and UPE/rGO composites. It can be seen from the figure that the thermal conductivity of UPE/NG, UPE/CNF, and UPE/rGO composites all increase with the increase of fillers; especially the thermal conductivity of UPE/NG composites increases most obviously. The thermal conductivity of UPE/NG composites has increased from 0.496 to 0.632 W/(mK) (5 phr NG), 0.749 W/(mK) (10 phr NG), 1.182 W/(mK) (20 phr NG), 2.200 W/(mK) (40 phr NG), and 3.257 W/(mK) (60 phr NG), an increase of 27.4, 51.0, 138.3, 343.5, and 556.7%, respectively. The increase in thermal conductivity is mainly attributed to the highly regular structure and high thermal conductivity of natural graphite. Not only can the heat conduction phonons transfer heat along the regular crystals of natural graphite, but also the conduction of electrons can transfer a large amount of heat. The added natural graphite is in a micron-size structure, and the interface thermal resistance is also very small. The combination of these will inevitably result in higher thermal conductivity. The thermal conductivity of UPE/CNF composites has also increased from 0.496 to 0.571 W/(mK) (5 phr CNF), 0.598 W/(mK) (10 phr CNF), 0.622 W/(mK) (20 phr CNF), 0.673 W/(mK) (40 phr CNF), and 0.778 W/(mK) (60 phr CNF), an increase of 14.7, 20.6, 25.4, 35.7 ,and 56.9%, respectively. The thermal conductivity of CNF is 1200 W/(mK), but this refers to the heat transfer of a single carbon fiber along the fiber axis. After the material is pressed into shape, many nano-carbon fibers do not transmit heat along the direction of heat conduction. After CNF is added to UPE material to form UPE/CNF composites, it can be seen from Figure 5b that CNF has a certain agglomeration phenomenon. From Figure 10b, it is found that the density of the material decreases with the increase of CNF content, which will greatly reduce the heat transfer of the material. The conductivity and thermal conductivity of rGO are much higher than those of NG and CNF, but the thermal conductivity of the UPE/rGO composite shown in Figure 11bchanged from 0.496 W/(mK) to 0.498 W/(mK) (5 phr rGO) and then to 0.520 W/(mK) (10 phr rGO); after that, there was almost no change. The thermal conductivity of rGO on the plane is the highest among the three fillers, but it is the lowest among UPE materials. The reasons for the low thermal conductivity are the chaotic arrangement of rGO, the great interface thermal resistance that hinders the heat transfer, and the volume expansion caused by the UPE/rGO composite during the formation process (the void in Figure 5f).

Figure 12 shows a diagram of the thermal conduction mechanism of composites. Combining Figures 5a,b and 12a, it

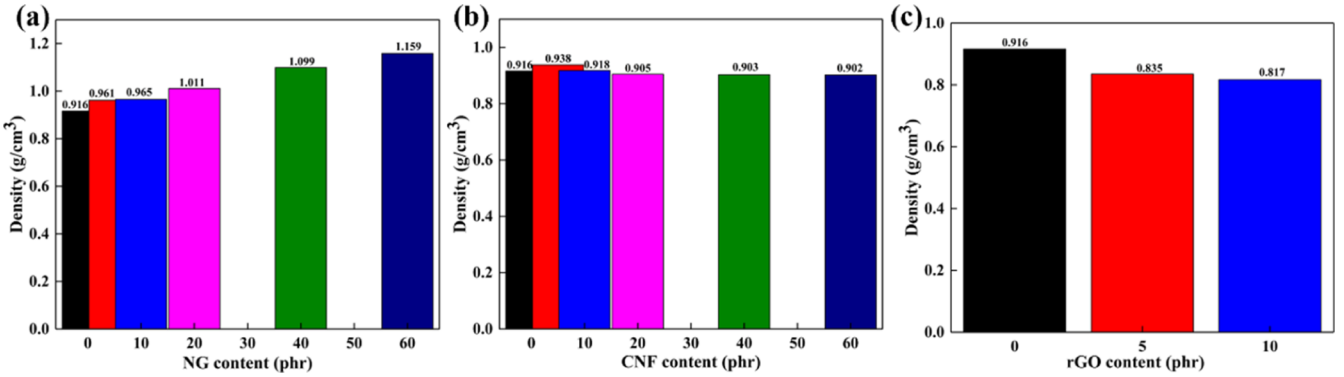

Figure 10. Density of composites. (a) Density of UPE/NG composites. (b) Density of UPE/CNF composites. (c) Density of UPE/rGO composites.

https://doi.org/10.1021/acsomega.1c07023
ACS Omega 2022, 7, 5547−5557

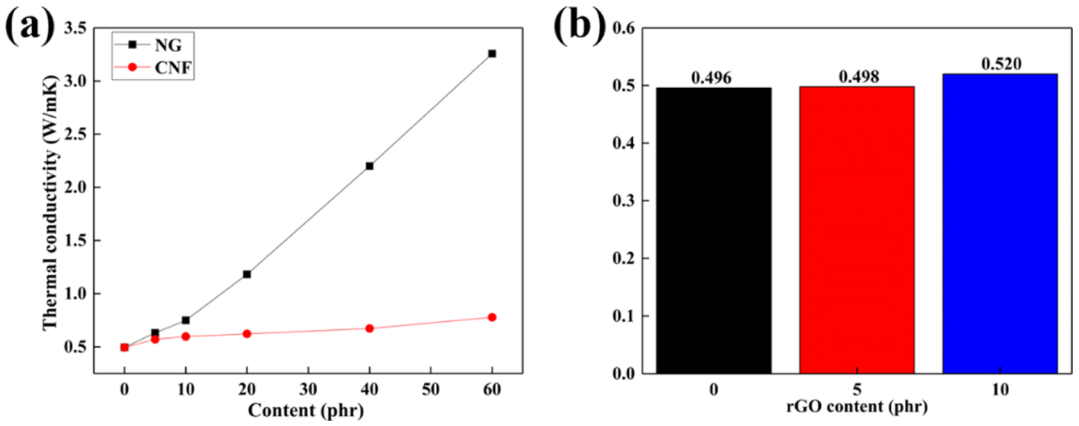

Figure 11. Thermal conductivity of composites. (a) Thermal conductivity of UPE/NG and UPE/CNF composites. (b) Thermal conductivity of UPE/rGO composites.

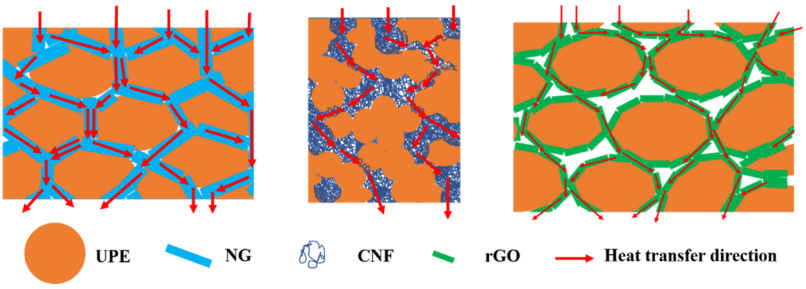

Figure 12. Schematic diagram of the heat flow transfer process in composites. (a) Heat flow transfer process of UPE/NG composites, (b) heat flow transfer process of UPE/CNF composites, and (c) heat flow transfer process of UPE/rGO composites.

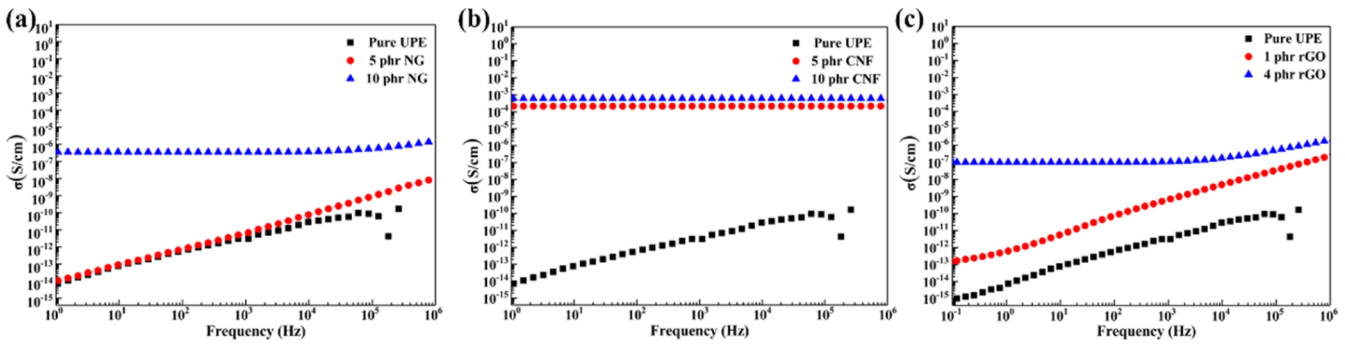

Figure 13. AC conductivity of composites. (a) AC conductivity of UPE/NG composites. (b) AC conductivity of UPE/CNF composites. (c) AC conductivity of UPE/rGO composites.

can be seen that UPE particles are tightly wrapped by NG particles, forming a honeycomb structure. The honeycomb structure greatly increases the contact probability of NG and increases the heat conduction path of UPE/NG composites. At the same time, heat can be conducted along the NG, which greatly increases the thermal conductivity, so the thermal conductivity of UPE/NG composites is higher. It can be seen from Figure 12a that some CNFs show an agglomerated phenomenon, which leads to less CNF content in some locations, reducing the heat conduction path and thus hindering the heat transfer efficiency. It can also be verified from the thermal conductivity test results that the thermal conductivity of UPE/CNF composites is low. It can be seen from Figure 12c that rGO is uniformly dispersed in UPE particles, and there are many gaps between UPE particles, which is very unfavorable for heat transfer. The rGO obtained by redox treatment becomes thinner and the interfacial thermal resistance between them increases, which leads to a poor thermal conductivity path. The increase in voids as well as the interfacial thermal resistance will make the UPE/rGO composite more likely to store heat rather than conduct it. This can also be verified from the thermal conductivity results. In summary, UPE/NG composites have the highest thermal conductivity, UPE/CNF composites have the second highest thermal conductivity, and UPE/rGO composites have the lowest thermal conductivity.

3.7. Conductive Properties of Composites. Figure 13 shows the AC conductivity of UPE/NG, UPE/CNF, and UPE/rGO composites. From Figure 13a, it can be found that the AC conductivity of UPE/NG (5 phr NG) composites and the AC conductivity curve of pure UPE material are superimposed. At 100 Hz, the AC conductivity of both is 10^{-14} S/cm order of magnitude. The AC conductivity of the UPE/NG (10% NG) composites has percolated, and the AC

https://doi.org/10.1021/acsomega.1c07023
ACS Omega 2022, 7, 5547−5557

conductivity curve has a plateau between 10^{-6} and 10^{-7} S/cm. From Figure 13b, it can be found that the AC conductivity of the UPE/CNF (5 phr CNF) composite has reached percolation. At 100 Hz, the AC conductivity is on the order of 10^{-4} S/cm. The AC conductivity of the UPE/CNF (10 phr CNF) composites has reached the order of 10^{-3} to 10^{-4} S/cm, the conductivity has been greatly improved, and the antistatic effect has been achieved. From Figure 13c, the addition of rGO (1 phr) can increase the AC conductivity. At 100 Hz, it reaches a level of 10^{-12} S/cm which is 2 orders of magnitude higher than that of pure UPE material. The AC conductivity of UPE/rGO (4 phr) composites has reached percolation, reaching a level of 10^{-7} S/cm at 100 Hz, which is similar to UPE/NG (10 phr NG) composites. It further shows that NG has been exfoliated into reduced GO material. In summary, the increasing order of AC conductivity is NG < rGO < CNF.

Figure 14 shows the DC conductivity of UPE/NG, UPE/CNF, and UPE/rGO composites. It can be seen from Figure 14 that in the three composites, the conductivity increases with the increase of the filler. The conductivity change of UPE/NG composites is 10^{-15} S/cm (5 phr NG), 3.5×10^{-7} S/cm (10 phr NG), 2.2×10^{-4} S/cm (20 phr NG), 1.08×10^{-2} S/cm (40 phr NG), and 1.93×10^{-2} S/cm (60 phr NG). The ratio of abrupt conductivity changes is 10%, and it can be found from the AC conductivity in Figure 13a that it has reached percolation. The conductivity of UPE/CNF composites is 2.0×10^{-4} S/cm (5 phr CNF), 6.0×10^{-4} S/cm (10 phr CNF), 1.03×10^{-2} S/cm (20 phr CNF), 2.59×10^{-2} S/cm (40 phr CNF), and 1.48×10^{-1} S/cm (60 phr CNF). The ratio of conductivity mutation is 5%, and it can be found from the AC conductivity in Figure 13b that it has reached percolation. The conductivity of UPE/rGO composites is 1×10^{-14} S/cm (1 phr rGO), 1.5×10^{-7} S/cm (4 phr rGO), 2.4×10^{-5} S/cm (5 phr rGO), and 1.5×10^{-4} S/cm (10 phr rGO). The ratio of conductivity mutation is 4%, and it can be found from the AC conductivity shown in Figure 13c that it has reached percolation. When the same 10% filler is used, the order of the DC conductivity of the composite is UPE/CNF > UPE/rGO > UPE/NG. The order of electrical conductivity is not the same as the order of thermal conductivity, indicating that the electrical and thermal conductivity mechanisms of composites are different. The conduction mechanism is electronic conduction, and electrons can easily cross the interface barrier and are not greatly affected by the interface. The heat conduction is mainly based on the heat conduction of phonons, and it is difficult for the heat conduction phonons to cross the interface barrier and is greatly affected by the interface.

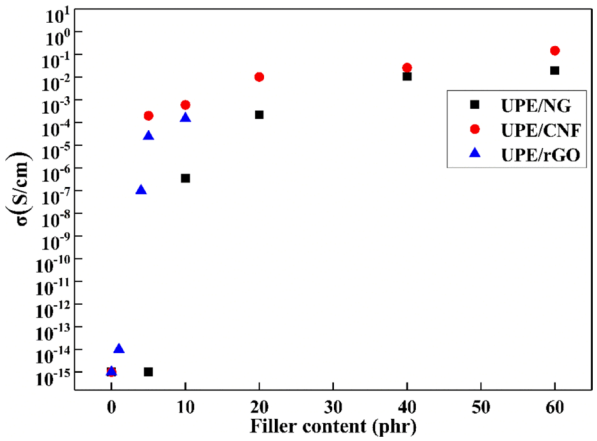

Figure 14. DC conductivity of UPE/NG, UPE/CNF, and UPE/rGO composites.

4. CONCLUSIONS

(1) The structure of the UPE/NG composites is regular, and the material density gradually increases with the increase of the filler. The structure of the UPE/CNF composites is still regular on the whole, but there is still a certain agglomeration phenomenon, but the TGA test shows that the material is relatively uniform and the density of the material does not change much. The density of UPE/rGO composites decreases with the increase of rGO, and there are many voids. The thermal conductivity of UPE/NG (60 phr NG) composites is 3.257 W/(mK), which is 556.7% higher than the thermal conductivity of pure UPE material of 0.496 W/(mK), and the electrical conductivity is greatly improved. The thermal conductivity of the UPE/CNF (60 phr CNF) composites is 0.778 W/(mK), which is 56.9% higher than that of pure UPE. The thermal conductivity of the UPE/rGO (10 phr rGO) composites is 0.52 W/(mK), which is similar to that of pure UPE. The thermal conductivity is related to the structure of the composites. The denser the composites and the more regular the thermally conductive crystal structure, the more conducive it is to the formation of the thermally conductive path.

(2) The order of thermal conductivity of UPE/NG, UPE/CNF, and UPE/rGO composites is UPE/NG > UPE/CNF > UPE/rGO. When the same 10 phr filler is used, the conductivity order of the composites is UPE/CNF > UPE/rGO > UPE/NG. The order of conductivity is not the same as the order of thermal conductivity, indicating that the electrical and thermal conductivity mechanisms of materials are different. The mechanism of conduction is electronic conduction, which is not too affected by the interface. The heat conduction mechanism is the percolation theory, and the heat conduction is mainly based on phonon conduction, supplemented by electron conduction, and it is greatly affected by the interface.

AUTHOR INFORMATION

Corresponding Authors

Xinfeng Wu − *Merchant Marine College, College of Ocean Science and Engineering, Shanghai Maritime University, Shanghai 201306, China; Shanghai Key Lab of Electrical Insulation and Thermal Aging and Department of Polymer Science and Engineering, Shanghai Jiao Tong University, Shanghai 200240, China;* orcid.org/0000-0002-8597-8272; Email: xfwu@shmtu.edu.cn

Wenge Li − *Merchant Marine College, College of Ocean Science and Engineering, Shanghai Maritime University, Shanghai 201306, China*; Email: wgli@shmtu.edu.cn

Jinhong Yu − *Key Laboratory of Marine Materials and Related Technologies, Zhejiang Key Laboratory of Marine Materials and Protective Technologies, Ningbo Institute of Materials Technology & Engineering, Chinese Academy of Sciences, Ningbo 315201, China;* orcid.org/0000-0001-9134-7568; Email: yujinhong@nimte.ac.cn

https://doi.org/10.1021/acsomega.1c07023
ACS Omega 2022, 7, 5547−5557

Authors

Yuantao Zhao − *Merchant Marine College, College of Ocean Science and Engineering, Shanghai Maritime University, Shanghai 201306, China*

Tao Jiang − *Merchant Marine College, College of Ocean Science and Engineering, Shanghai Maritime University, Shanghai 201306, China;* orcid.org/0000-0002-6631-2192

Ying Wang − *Merchant Marine College, College of Ocean Science and Engineering, Shanghai Maritime University, Shanghai 201306, China*

Pingkai Jiang − *Shanghai Key Lab of Electrical Insulation and Thermal Aging and Department of Polymer Science and Engineering, Shanghai Jiao Tong University, Shanghai 200240, China*

Shanshan Shi − *Merchant Marine College, College of Ocean Science and Engineering, Shanghai Maritime University, Shanghai 201306, China*

Kai Sun − *Merchant Marine College, College of Ocean Science and Engineering, Shanghai Maritime University, Shanghai 201306, China;* orcid.org/0000-0001-7396-5813

Bo Tang − *Hangzhou Vulcan New Materials Technology Co., Ltd, Hangzhou 311255, China*

Complete contact information is available at: https://pubs.acs.org/10.1021/acsomega.1c07023

Author Contributions

⊥Y.Z., T.J., and Y.W. contributed equally.

Notes

The authors declare no competing financial interest.

■ ACKNOWLEDGMENTS

This work was financially supported by the Project Funded by China Postdoctoral Science Foundation (2017M611757), the Special Fund of the National Natural Science Foundation of China (51573201and 51803119) and Shanghai High-level Local University Innovation Team (Maritime safety & technical support).

■ REFERENCES

(1) Patel, K.; Chikkali, S. H.; Sivaram, S. Ultrahigh molecular weight polyethylene: Catalysis, structure, properties, processing and applications. *Prog. Polym. Sci.* **2020**, *109*, 101290.

(2) Gilman, A. B.; Piskarev, M. S.; Kuznetsov, A. A.; Ozerin, A. N. Modification of ultrahigh-molecular-weight polyethylene by low-temperature plasma (review). *High Energy Chem.* **2017**, *51*, 136−144.

(3) Zhang, H.; Zhao, S.; Xin, Z.; Ye, C.; Li, Z.; Xia, J. Wear Resistance Mechanism of Ultrahigh-Molecular-Weight Polyethylene Determined from Its Structure-Property Relationships. *Ind. Eng. Chem. Res.* **2019**, *58*, 19519−19530.

(4) Wang, H.; Quan, J.; Yu, J.; Zhu, J.; Wang, Y.; Hu, Z. Enhanced wear resistance of ultra-high molecular weight polyethylene fibers by modified-graphite oxide. *J. Appl. Polym. Sci.* **2021**, *138*, 50696.

(5) Zhang, Z.; Ren, S. Functional Gradient Ultrahigh Molecular Weight Polyethylene for Impact-Resistant Armor. *ACS Appl. Polym. Mater.* **2019**, *1*, 2197−2203.

(6) Li, C.; Zhang, R.; Jia, J.; Wang, G.; Shi, Y. The low-velocity impact and post-impact properties of ultra-high-molecular-weight polyethylene fiber weft plain knitted structural composites. *J. Eng. Fibers Fabr.* **2019**, *14*, 1558925019832524.

(7) Aliyu, I. K.; Mohammed, A. S. Wear and corrosion resistance performance of UHMWPE/GNPs nanocomposite coatings on AA2028 Al alloys. *Prog. Org. Coat.* **2021**, *151*, 106072.

(8) Adesina, A. Y.; Khan, M. F.; Azam, M. U.; Abdul Samad, M.; Sorour, A. A. Characterization and corrosion resistance of ultra-high molecular weight polyethylene composite coatings reinforced with tungsten carbide particles in hydrochloric acid medium. *J. Polym. Eng.* **2019**, *39*, 861−873.

(9) Candadai, A. A.; Weibel, J. A.; Marconnet, A. M. Thermal Conductivity of Ultrahigh Molecular Weight Polyethylene: From Fibers to Fabrics. *ACS Appl. Polym. Mater.* **2019**, *2*, 437−447.

(10) Huang, Y.-F.; Wang, Z.-G.; Yu, W.-C.; Ren, Y.; Lei, J.; Xu, J.-Z.; Li, Z.-M. Achieving high thermal conductivity and mechanical reinforcement in ultrahigh molecular weight polyethylene bulk material. *Polymer* **2019**, *180*, 121760.

(11) Wang, X.; Feng, C. P.; Wang, M.; Lu, H.; Ni, H. Y.; Chen, J. Multilayered ultrahigh molecular weight polyethylene/natural graphite/boron nitride composites with enhanced thermal conductivity and electrical insulation by hot compression. *J. Appl. Polym. Sci.* **2020**, *138*, 49938.

(12) Guo, Y.; Cao, C.; Luo, F.; Huang, B.; Xiao, L.; Qian, Q.; Chen, Q. Largely enhanced thermal conductivity and thermal stability of ultra high molecular weight polyethylene composites via BN/CNT synergy. *RSC Adv.* **2019**, *9*, 40800−40809.

(13) Shi, A.; Li, Y.; Liu, W.; Xu, J.-Z.; Yan, D.-X.; Lei, J.; Li, Z.-M. Highly thermally conductive and mechanically robust composite of linear ultrahigh molecular weight polyethylene and boron nitride via constructing nacre-like structure. *Compos. Sci. Technol.* **2019**, *184*, 107858.

(14) Berenguer, J. P.; Berman, A.; Quill, T.; Zhou, T.; Kalaitzidou, K.; Cola, B.; Bougher, T.; Smith, M. Incorporation of polyethylene fillers in all-polymer high-thermal-conductivity composites. *Polym. Bull.* **2020**, *78*, 3835−3850.

(15) Liu, H.; Yu, X.; Ji, M.; Chen, H.; Yang, G.; Zhu, C.; Xu, J. High through-plane thermal conductivity and light-weight of UHMWPE fibers/PDMS composites by a large-scale preparation method. *Polymer* **2021**, *229*, 123975.

(16) Shi, A.; Li, Y.; Liu, W.; Lei, J.; Li, Z.-M. High thermal conductivity of chain-aligned bulk linear ultra-high molecular weight polyethylene. *J. Appl. Phys.* **2019**, *125*, 245110.

(17) Han, L.; Cai, H.; Chen, X.; Zheng, C.; Guo, W. Study of UHMWPE Fiber Surface Modification and the Properties of UHMWPE/epoxy Composite. *Polymers* **2020**, *12*, 521.

(18) Wang, X.; Lu, H.; Feng, C.; Ni, H.; Chen, J. Facile method to fabricate highly thermally conductive UHMWPE/BN composites with the segregated structure for thermal management. *Plast., Rubber Compos.* **2020**, *49*, 196−203.

(19) Wang, Z. Y.; Zhou, X. N.; Li, Z. X.; Xu, S. S.; Hao, L. C.; Zhao, J. P.; Wang, B.; Yang, J. F.; Ishizaki, K. Enhanced thermal conductivity of epoxy composites by constructing thermal conduction networks via adding hybrid alumina filler. *Polym. Compos.* **2021**, *43*, 483.

(20) Feng, C. P.; Chen, L.; Wei, F.; Ni, H. Y.; Chen, J.; Yang, W. Highly thermally conductive UHMWPE/graphite composites with segregated structures. *RSC Adv.* **2016**, *6*, 65709−65713.

(21) Nayak, S. K.; Mohanty, S.; Nayak, S. K. A new way synthesis of expanded graphite as a thermal filler to enhance the thermal conductivity of DGEBA resin as thermal interface material. *High Perform. Polym.* **2019**, *32*, 506−523.

(22) Mazo, M. A.; Tamayo, A.; Caballero, A. C.; Rubio, J. Enhanced electrical and thermal conductivities of silicon oxycarbide nanocomposites containing carbon nanofibers. *Carbon* **2018**, *138*, 42−51.

(23) Ma, X.; Wang, W.-y.; Qi, X.-d.; Yang, J.-h.; Lei, Y.-z.; Wang, Y. Highly thermally conductive epoxy composites with anti-friction performance achieved by carbon nanofibers assisted graphene nanoplatelets assembly. *Eur. Polym. J.* **2021**, *151*, 110443.

(24) Zhuang, C.; Tao, R.; Liu, X.; Zhang, L.; Cui, Y.; Liu, Y.; Zhang, Z. Enhanced thermal conductivity and mechanical properties of natural rubber-based composites co-incorporated with surface treated alumina and reduced graphene oxide. *Diamond Relat. Mater.* **2021**, *116*, 108438.

(25) Cheng, S.; Duan, X.; Zhang, Z.; An, D.; Zhao, G.; Liu, Y. Preparation of a natural rubber with high thermal conductivity, low

heat generation and strong interfacial interaction by using NS-modified graphene oxide. *J. Mater. Sci.* **2020**, *56*, 4034−4050.
(26) Wu, X.; Tang, B.; Chen, J.; Shan, L.; Gao, Y.; Yang, K.; Wang, Y.; Sun, K.; Fan, R.; Yu, J. Epoxy composites with high cross-plane thermal conductivity by constructing all-carbon multidimensional carbon fiber/graphite networks. *Compos. Sci. Technol.* **2021**, *203*, 108610.
(27) Ruan, K.; Shi, X.; Guo, Y.; Gu, J. Interfacial thermal resistance in thermally conductive polymer composites: A review. *Compos. Commun.* **2020**, *22*, 100518.
(28) Li, M.; Li, L.; Hou, X.; Qin, Y.; Song, G.; Wei, X.; Kong, X.; Zhang, Z.; Do, H.; Greer, J. C.; Han, F.; Cai, T.; Dai, W.; Lin, C.-T.; Jiang, N.; Yu, J. Synergistic effect of carbon fiber and graphite on reducing thermal resistance of thermal interface materials. *Compos. Sci. Technol.* **2021**, *212*, 108883.
(29) Feng, C.-P.; Bai, L.; Shao, Y.; Bao, R.-Y.; Liu, Z.-Y.; Yang, M.-B.; Chen, J.; Ni, H.-Y.; Yang, W. A Facile Route to Fabricate Highly Anisotropic Thermally Conductive Elastomeric POE/NG Composites for Thermal Management. *Adv. Mater. Interfac.* **2018**, *5*, 1700946.
(30) Ruiz-Cornejo, J. C.; Sebastián, D.; Lázaro, M. J. Synthesis and applications of carbon nanofibers: a review. *Rev. Chem. Eng.* **2020**, *36*, 493−511.
(31) Yadav, D.; Amini, F.; Ehrmann, A. Recent advances in carbon nanofibers and their applications-A review. *Eur. Polym. J.* **2020**, *138*, 109963.
(32) Yin, F.; Hu, J.; Hong, Z.; Wang, H.; Liu, G.; Shen, J.; Wang, H.-L.; Zhang, K.-Q. A review on strategies for the fabrication of graphene fibres with graphene oxide. *RSC Adv.* **2020**, *10*, 5722−5733.
(33) Ullah, S.; Yang, X.; Ta, H. Q.; Hasan, M.; Bachmatiuk, A.; Tokarska, K.; Trzebicka, B.; Fu, L.; Rummeli, M. H. Graphene transfer methods: A review. *Nano Res.* **2021**, *14*, 3756−3772.
(34) Jin, Z.; E, S.; Luo, Z.; Ning, D.; Huang, J.; Ma, Q.; Jia, F.; Lu, Z. Investigations on the thermal conduction behaviors of reduced graphene oxide/aramid nanofibers composites. *Diamond Relat. Mater.* **2021**, *116*, 108422.
(35) Liu, C.; Wu, W.; Wang, Y.; Liu, X.; Chen, Q.; Xia, S. Silver Nanoparticle-Enhanced Three-Dimensional Boron Nitride/Reduced Graphene Oxide Skeletons for Improving Thermal Conductivity of Polymer Composites. *ACS Appl. Polym. Mater.* **2021**, *3*, 3334−3343.

https://doi.org/10.1021/acsomega.1c07023
ACS Omega 2022, 7, 5547−5557